

Van der Waals epitaxy growth of 2D ferromagnetic $\text{Cr}_{(1+\delta)}\text{Te}_2$ nanolayers with concentration-tunable magnetic anisotropy


F

Cite as: Appl. Phys. Rev. 9, 011409 (2022); <https://doi.org/10.1063/5.0070079>

Submitted: 03 September 2021 • Accepted: 04 January 2022 • Published Online: 21 January 2022

 Kinga Lasek, Paula M. Coelho,  Pierluigi Gargiani, et al.

COLLECTIONS

 This paper was selected as Featured

[View Online](#)[Export Citation](#)[CrossMark](#)

Applied Physics
Reviews

Read. Cite. Publish. Repeat.

19.162

2020 IMPACT FACTOR*

Van der Waals epitaxy growth of 2D ferromagnetic $\text{Cr}_{(1+\delta)}\text{Te}_2$ nanolayers with concentration-tunable magnetic anisotropy

Cite as: Appl. Phys. Rev. **9**, 011409 (2022); doi: [10.1063/5.0070079](https://doi.org/10.1063/5.0070079)

Submitted: 3 September 2021 · Accepted: 4 January 2022 ·

Published Online: 21 January 2022










View Online



Export Citation



CrossMark

Kinga Lasek,^{1,a)}  Paula M. Coelho,¹ Pierluigi Gargiani,²  Manuel Valvidares,²  Katayoon Mohseni,³ 
Holger L. Meyerheim,³  Ilya Kostanovskiy,³ Krzysztof Zborecki,⁴  and Matthias Batzill¹ 

AFFILIATIONS

¹Department of Physics, University of South Florida, Tampa, Florida 33620, USA

²ALBA Synchrotron Light Source, E-08290 Cerdanyola del Vallès, Barcelona, Spain

³Max-Planck-Institut für Mikrostrukturphysik, Weinberg 2, D-06120 Halle, Germany

⁴Faculty of Physics, Warsaw University of Technology, ul. Koszykowa 75, Warsaw 00-662, Poland

^{a)} Author to whom correspondence should be addressed: klasek@usf.edu

ABSTRACT

$\text{Cr}_{(1+\delta)}\text{Te}_2$ are pseudo-layered compounds consisting of CrTe_2 transition metal dichalcogenide (TMD) layers with additional (δ) self-intercalated Cr atoms. The recent search for ferromagnetic 2D materials revived the interest into chromium tellurides. Here, $\text{Cr}_{(1+\delta)}\text{Te}_2$ nanolayers are epitaxially grown on MoS_2 (0001), forming prototypical van der Waals heterostructures. Under optimized growth conditions, ultrathin films of only two TMD layers with a single intercalated Cr-layer are achieved, forming a 2D sheet with van der Waals surfaces. Detailed compositional and structural characterization by scanning tunneling microscopy, grazing incidence x-ray diffraction, and high-resolution Rutherford backscattering indicate the layer-by-layer growth and that the δ can be tuned by post-growth annealing in a range between ~ 0.5 and 1. X-ray magnetic circular dichroism and magnetometry measurements demonstrate that all self-intercalated $\text{Cr}_{(1+\delta)}\text{Te}_2$ nanolayers exhibit strong ferromagnetism with magnetic moments larger than $3\mu_B$ per Cr-atom. The magnetic properties are maintained in the ultrathin limit of a material with a single intercalation layer. Interestingly, the magnetic anisotropy can be tuned from close to isotropic ($\delta = 1$) to a desirable perpendicular anisotropy for low δ values. Thus, the bottom-up growth of these 2D $\text{Cr}_{(1+\delta)}\text{Te}_2$ sheets is a promising approach for designing magnetic van der Waals heterostructures.

Published under an exclusive license by AIP Publishing. <https://doi.org/10.1063/5.0070079>

I. INTRODUCTION

Magnetic van der Waals (vdW) materials hold promise for their potential in spintronic devices by combining them with other vdW materials with atomically sharp interfaces.^{1,2} Such vdW heterostructures may be prepared by exfoliation and mechanical stacking, which requires bulk vdW materials that can be exfoliated.³ Most of the available magnetic vdW materials are, however, chemically sensitive, thus making their handling challenging. Moreover, mechanical stacking approaches are inherently non-scalable processes and, thus, not suitable beyond fundamental investigations. Therefore, development and understanding of bottom-up growth processes of vdW heterostructures are important for scalable materials synthesis of magnetic vdW systems.⁴ The choices of ferromagnetic vdW crystals are still very limited, and most of them have low Curie temperatures.^{1,3} The bottom-up growth by molecular beam epitaxy (MBE) also enables the

combination of vdW materials with non-vdW materials, commonly referred to as vdW epitaxy. Such systems exhibit a vdW gap at the interface, i.e., an interface without covalent bonding between the materials. VdW epitaxy has been well documented for the growth of lattice mismatched vdW materials on non-vdW substrates.^{5–11} The low surface energy and the large two-dimensional (2D) anisotropy of the crystal structure inherent to vdW materials assist the layer-by-layer growth in these systems. Here, we explore the bottom-up growth of $\text{Cr}_{(1+\delta)}\text{Te}_2$, a material closely related to vdW materials. It consists of 2D- CrTe_2 sheets but with additional Cr-atoms interspersed between these molecular sheets that covalently link the two TMD sheets together. Although these additional Cr-atoms in between CrTe_2 layers are often referred to as a self-intercalation layer, it is important to point out that the Cr-atoms in this layer are covalently bound to six next neighbor Te-atoms in the TMD layers and, thus, have the same

coordination as Cr atoms within the TMD layers. This makes all the Cr-atoms in the $\text{Cr}_{(1+\delta)}\text{Te}_2$ compounds chemically similar. We demonstrate that these materials can also be grown by vdW epitaxy on a dissimilar vdW substrate (MoS_2),¹² and under optimized growth conditions, the ultrathin limit of a bilayer CrTe_2 with a single Cr-intercalation layer can be prepared.

The chromium-telluride system has several magnetic phases.¹³ Recently, the layered transition metal dichalcogenide, 1T- CrTe_2 , was synthesized and it was shown to exhibit ferromagnetic properties in the bulk,¹⁴ as a thin film,^{15,16} and in the form of exfoliated flakes.^{17–19} However, this material is only metastable and disproportionates into elemental Te and stable $\text{Cr}_{(1+\delta)}\text{Te}_2$ intercalation compounds upon annealing.¹⁴ These (self) intercalation compounds exist in different compositional phases that vary by the amount of Cr intercalated between CrTe_2 layers.²⁰ The variation of the amount of intercalated Cr is represented by δ , which indicates the fraction of intercalated Cr compared to the amount of Cr in a CrTe_2 -TMD layer. These compounds have been prepared in the form of bulk crystals²¹ and as epitaxial films^{22–26} to study their (ferro-) magnetic properties. It was shown that the Curie temperature of these materials vary significantly from 160 K to above room temperature depending on the film thickness,^{27,28} post-growth annealing temperature,¹³ and the Te: Cr flux ratio.²⁹ In the current report, we characterize the structure and composition of the films in detail in order to better understand the interplay between magnetic properties and growth conditions. Specifically, we show that the amount of self-intercalated Cr can be controlled by post-growth annealing, which affects the magnetic anisotropy of the material. Importantly, we demonstrate that ultrathin vdW films can be prepared with the ultimate limit of a single self-intercalated layer by vdW epitaxy. These vdW materials maintain their ferromagnetic properties with desirable out-of-plane anisotropy and, thus, are potential ferromagnetic (pseudo) 2D materials that can be combined in vdW heterostructures by a bottom-up growth process.

II. EXPERIMENTAL SECTION

A. Growth

The $\text{Cr}_{(1+\delta)}\text{Te}_2$ films were grown by co-deposition of chromium and tellurium in an ultra-high vacuum MBE chamber on synthetically grown, commercial single crystalline MoS_2 substrates. The substrates were freshly cleaved in air and subsequently outgassed in vacuum at 300 °C for at least two hours before growth. Cr was evaporated from a mini e-beam evaporator while Te was co-deposited from a Knudsen cell. The Te- and Cr- deposition rates were calibrated with a quartz microbalance to about 0.15 and 0.015 nm/min, respectively. The substrate temperature during growth was set to 200 °C or to 350 °C for the low- or high-temperature growth discussed below. Post-growth annealing was carried out in a temperatures range of 400 °C–500 °C.

B. Surface characterization

After the growth, samples are transferred *in situ* from the MBE chamber to a surface analysis chamber. Large scale and atomically resolved images were obtained at room temperature using an Omicron STM-1 with electrochemically etched tungsten tips. The surface crystal periodicity of the grown film is evaluated from low energy electron diffraction (LEED) diffraction patterns measured at the electron beam energy of 55–70 eV. Ultraviolet photoemission

spectroscopy (UPS) characterization of the valence band was carried out with a He-I vacuum ultraviolet excitation source and a Scienta R3000 hemispherical electron energy analyzer.

C. Structural and compositional characterization

Grazing incidence x-ray diffraction (GIXRD) was performed using a gallium-jet x-ray source operated at 70 keV and 100 W power emitting Ga-K α radiation ($\lambda = 0.13414$ nm) and a six-circle x-ray diffractometer especially designed for the study of ultra-thin films and interfaces. In this setup, the monochromatized and focused x-ray beam (horizontal and vertical beam size: $2\text{ mm} \times 100\ \mu\text{m}$) is incident onto the sample at a constant grazing incidence angle of $\mu = 2^\circ$. Additional experimental details and data analysis are described in the [supplementary material](#), Sec. I.

Rutherford backscattering spectroscopy (RBS) characterization of the $\text{Cr}_{(1+\delta)}\text{Te}_2$ thin film samples was carried out with a He⁺-beam produced by the commercial NEC Pelletron ion accelerator. An ion beam of 1.9 MV and 40 nA current was hitting the sample tilted by 9° in order to avoid channeling geometry. Backscattered spectra were collected by the Amptek implanted detector with an energy resolution of 16 keV at 169° scattering angle. For samples protected with a Te capping layer, Te from the capping layer could not be separated from those of the film and, thus, compositional analysis was not possible with regular RBS. Thus, some additional samples were capped with Pt, which allowed compositional analysis. In addition, Te-capped samples were studied with high resolution RBS (HRBS), measured in a commercial HRBS detection system (NEC), that consists of the magnetic spectrometer and a 10 cm multichannel plate (MCP) detector. HRBS data were collected with the 400 keV He⁺ beam energy, at which the backscattering cross section is close to its maximum. The HRBS geometry is fixed at 90° scattering angle, and low beam energy improves surface sensitivity as compared with regular RBS measurement. The incident and reflected angles of the beam to sample were 45° . Additional experimental details and data analysis of RBS/HRBS can be found in the [supplementary material](#), Sec. II.

D. Magnetic characterization

X-ray absorption spectroscopy (XAS) and x-ray magnetic circular dichroism (XMCD) measurements were performed at BL29 BOREAS at the ALBA synchrotron in Barcelona, Spain,³⁰ in the high-field magnet HECTOR end-station. The XAS signal was measured in total electron yield (TEY) mode at the Cr L_{2,3} edge with fully circularly or linearly polarized x-rays produced by an APPLE-II type undulator. The signal was normalized to the impinging photon flux measured by the TEY from a freshly evaporated gold mesh. The XMCD spectrum was obtained from the difference between XAS spectra measured with impinging x rays with left and right helicities. XMCD measurements were performed in an applied field of up to 6 T collinear to the beam direction, generated by a vector-type cryomagnet (Scientific Magnetics). The element-specific M-H loops were collected at the energy of the XMCD intensity maximum while continuously varying the applied field. The sample temperature varied between 2 and 300 K as measured on the cryostat cold finger a few centimeters away from the sample. To evaluate the Curie temperature (T_c), magnetization vs temperature measurements were carried out. The samples were cooled to 2 K with an applied field of 6 T, and the magnetization was

measured with an applied 0.05 mT field while warming up. The samples for the XAS/XMCD experiment were protected from air exposure during transfer by a Te capping layer. The initial XAS spectra revealed a tellurium oxide layer. The thermal stability of TeO_x required removing of the oxide by ion sputtered with 1 keV Ar^+ ions for 3–5 min. After removal of the oxide the remaining Te cap was thermally desorbed by annealing at 200 °C for 30 min. After this treatment, a clear Cr $L_{2,3}$ XAS signal could be measured.

In addition to XMCD, magnetic properties were also measured in a vibrating sample magnetometer (VSM) in a Quantum Design PPMS system. All the hysteresis loops were measured with an applied field ± 50 kOe after cooling in zero field. For zero field cooled (ZFC) magnetization vs temperature measurements, sample was cooled in zero field to 5 K from 300 K and the measurement was conducted with a 100 mT of an applied field while warming up. The field cooled (FC) curve was measured after ZFC curves while cooling down.

E. Calculations

All the calculations were performed within density functional theory (DFT) as implemented in the Vienna *Ab Initio* Simulation Package (VASP) code^{31–34} with Projector augmented wave pseudopotentials^{35,36} and PBE³⁷ (GGA) functional. For the sampling of the Brillouin zone, a dense $30 \times 30 \times 1$ grid was used, while the plane wave energy cutoff was set to 500 eV.

III. RESULTS

$\text{Cr}_{(1+\delta)}\text{Te}_2$ films are grown by MBE, by co-deposition of Cr and Te on the (0001) surface of a freshly cleaved, synthetically grown MoS_2 crystal. The grown films are transferred from a vacuum growth chamber by an *in situ* vacuum transfer to a surface analysis ultra-high vacuum (UHV) system for LEED and scanning tunneling microscopy (STM) characterization. To perform *ex situ* high resolution GIXRD, VSM, and XAS/XMCD characterization, the films are capped with a protective Te layer. To perform compositional analysis by RBS, films were also capped with Pt.

The results section is organized as follows: We first discuss the film morphology and composition as a function of the growth conditions, which shows that layer-by-layer growth is obtained at low growth temperatures close to 200 °C. We show that post growth annealing above 400 °C causes loss of Te and an increase in the Cr:Te ratio. We then apply the lower temperature growth condition to demonstrate the synthesis of ultrathin quasi 2D materials. Structural and compositional film characterization is related to the magnetic properties, which are investigated by XMCD and VSM. The latter provides evidence that the prepared films are ferromagnetic with a large magnetic moment ($\sim 3 \mu\text{B}/\text{Cr-atom}$), and their magnetic properties and magnetic anisotropy can be varied by the preparation conditions or post-growth annealing. These magnetic properties are related to their structural and compositional properties.

A. Van der Waals epitaxy of $\text{Cr}_{(1+\delta)}\text{Te}_2$

The main characteristic of vdW heterostructures is that the two crystalline layers that make up the heterostructure only weakly interact with each other. Consequently, the film grows fully relaxed and keeps its lattice constant and misfit-defects at the substrate-film interface are avoided. Here, we show that growth of $\text{Cr}_{(1+\delta)}\text{Te}_2$ on MoS_2 satisfies

these conditions and that the lattice vectors of the substrate and the $\text{Cr}_{(1+\delta)}\text{Te}_2$ layer are parallel to each other, i.e., the film exhibits an epitaxial relationship with the single-crystal substrate, thus avoiding the formation of rotational twist grains.

Film growth is carried out under excess Te flux of $\sim 10:1$ with respect to Cr. Thus, lowering the growth temperature is limited by the sticking of Te on the substrate surface at low temperatures. All films discussed here were grown in a temperature window between 200 °C and 400 °C. Once grown, some films were annealed to higher temperatures up to 500 °C to induce compositional changes related to the loss of tellurium.

Figure 1 shows a typical film grown at 200 °C. In the large-scale STM images [Fig. 1(a)], atomically flat terraces are observed with step heights of 0.6 nm between them [see line scan inset of Fig. 1(a)]. The LEED pattern [Fig. 1(d)] shows diffraction spots of both the MoS_2 substrate and of the film. From the LEED pattern, it is evident that the reciprocal lattice vectors of film and substrate are parallel. From the line scan shown in the inset, the first order reflection position of the film is at a position of approximately 0.82 reciprocal lattice units (rlu) of that of the MoS_2 substrate (lattice parameter $a_0 = b_0 = 0.316 \text{ nm}$)³⁸ corresponding to a film lattice parameter of $a = 0.386 \text{ nm}$ (see also x-ray diffraction analysis in the [supplementary material](#)) close to the bulk value of Cr_3Te_4 of $a = 0.394 \text{ nm}$.³⁹

Moreover, from the large scale STM image no indication of lattice mismatch induced dislocations or twist grain boundaries are observed. Consequently, we conclude that the $\text{Cr}_{(1+\delta)}\text{Te}_2$ film grows in a vdW epitaxy mode. The diffraction pattern of the film shows superstructure reflections corresponding to an apparent 2×2 periodicity in contrast to the 1×1 periodicity expected from a hexagonal 2D-TMD layer. Atomically resolved images [Figs. 1(b) and 1(c)] show that the surface exhibits a 2×1 periodicity with three equivalent rotational domains [two domains are shown in Fig. 1(b)]. The lower symmetry of the ordering of the Cr-atoms in the self-intercalation layer compared to the TMD layer gives rise to the 2×1 domains. Thus, these domains and their associated domain boundaries are only within the Cr-intercalation layer, while the TMD layers are contiguous without boundaries. A 2×1 periodicity is expected for a film with a Cr_3Te_4 stoichiometry, as illustrated in Fig. 1(e). This corresponds to $\delta = 0.5$ in the $\text{Cr}_{(1+\delta)}\text{Te}_2$ nomenclature. By contrast, the more commonly discussed Cr_2Te_3 ($\delta = 1/3$) stoichiometry for MBE grown Cr-Te films would exhibit a $(\sqrt{3} \times \sqrt{3}) R30^\circ$ structure. These structures and the corresponding calculated STM images are schematically illustrated in Fig. 1(e), with the $(\sqrt{3} \times \sqrt{3}) R30^\circ$ structure of Cr_2Te_3 exhibiting a much smaller expected corrugation than the 2×1 structure of Cr_3Te_4 .

A study of the film morphology as a function of sample preparation conditions is shown in Fig. 2. Generally, low temperature growth at around 200 °C results in much flatter surfaces and this is also shown in Fig. 2(a) by the STM image of a few (5–7) TMD-layer thick film, where we define the film thickness in terms of the number of CrTe_2 TMD layers. However, the LEED reflections appear more diffuse, suggesting a poor long-range order in the film. Annealing of such low temperature grown films does not induce any roughening of the film, and the LEED spots become sharper when the film is annealed at 400 °C. This indicates an ordering of the film. Samples annealed to 500 °C [Fig. 2(c)] exhibit less well-defined 2×1 reconstructed domains in STM, while the LEED pattern has not changed qualitatively. The less pronounced 2×1 domain structure in STM may

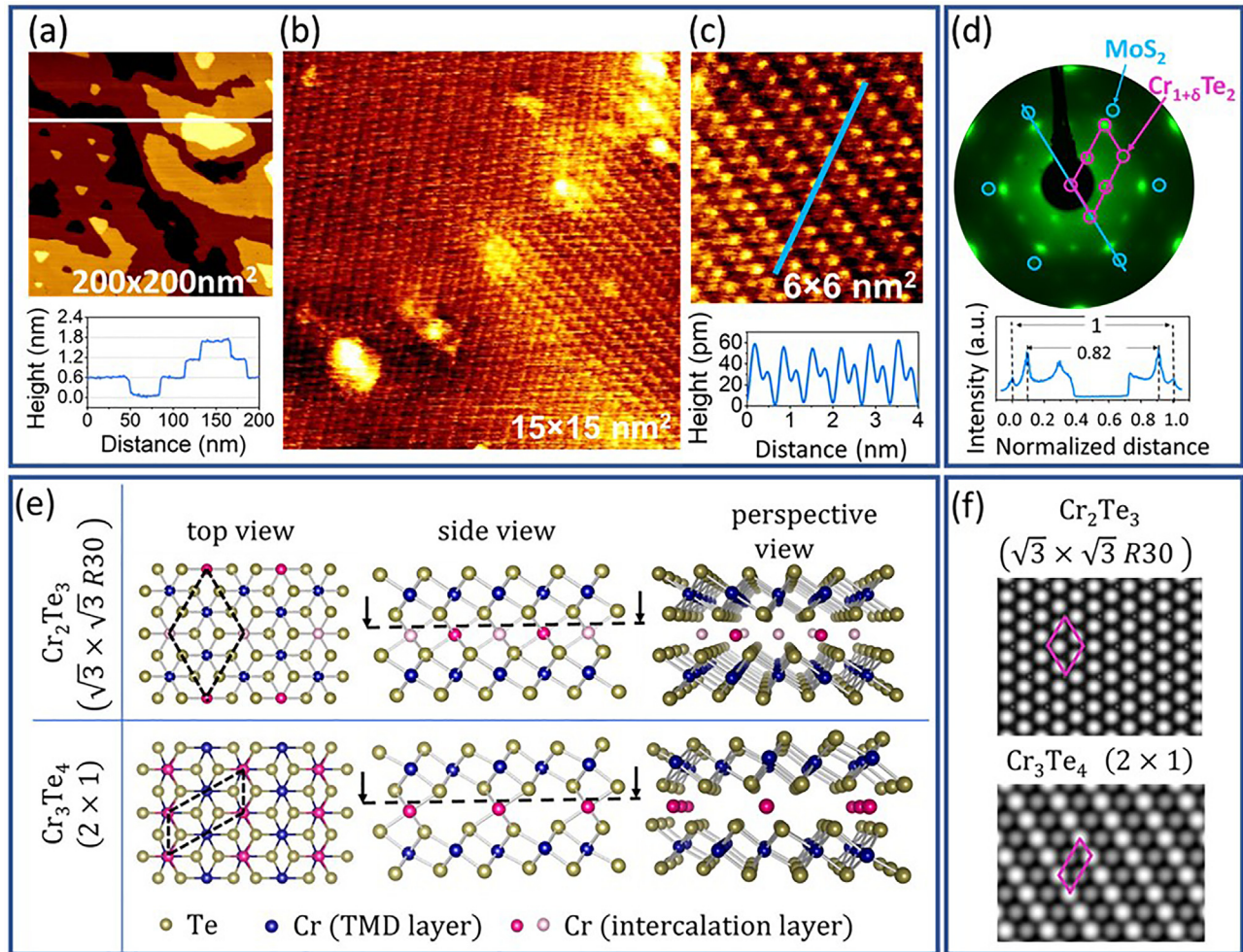


FIG. 1. Crystal structure, STM, and LEED characterization of a few-layer thick Cr-Te film grown on the MoS₂ substrate. (a) Large scale (200 × 200 nm²) STM image showing atomically flat terraces separated by steps of about 0.6 nm height. (b) and (c) High-resolution STM revealing two rotational domains of 2 × 1 periodicity. The maximum topographic corrugation is equal to about 0.03 nm. STM images are in agreement with the apparent 2 × 2 LEED pattern in (d), which corresponds to a (2 × 1) superlattice with three domains. The LEED pattern has been measured on the 3–4 layers thick film, with a primary electron energy of $E_k = 65$ eV. The lattice constant of Cr-Te film is measured by using the MoS₂ substrate diffraction spots as a reference, as shown in (d). STM imaging conditions (sample bias, tunneling current): (a) −1.2 V, 0.7 nA; (b) 5 mV, 0.9 nA. (e) Structure models of films with Cr₂Te₃ ($\sqrt{3} \times \sqrt{3} R30^\circ$) and Cr₃Te₄ (2 × 1) stoichiometry. The top view models are shown from the plane indicated by the dotted line in the side view figure. (f) Simulated STM images calculated for a relaxed bilayer structure with Cr-intercalation in Cr₂Te₃ and Cr₃Te₄ structures, illustrating that the intercalated atoms cause significant changes in the top TMD layer allowing its observation in STM.

indicate a disordering of the intercalated Cr-layer or more likely a compositional change in the Cr-intercalated layer due to the desorption of Te at elevated annealing temperature. Below we use RBS to show the increase in the δ in Cr_(1+ δ)Te₂ for annealed samples.

In contrast to the very flat films obtained by annealing of low temperature grown films, films that are grown directly at elevated temperatures (350 °C) expose significantly more terraces within the same imaging area. For a six TMD-layer thick film, at least five different terrace heights are observed within the 400 × 400 nm² imaging area, as shown in Fig. 2(d). This indicates that these high-temperature grown films are not of uniform thickness, but rather exposes local film thicknesses that at least vary by five TMD layers. Consistent with the exposure of many terraces is the observation that LEED reflections related

to the MoS₂ substrate are more pronounced, suggesting that some substrate regions may remain exposed or covered by only a very thin Cr_(1+ δ)Te₂ layer. The LEED reflections of the film are, however, very sharp, indicating that crystal structure of the film has a well-defined long-range order. Again, the film exhibits a 2 × 1 superstructure. The exposure of more terraces in the film may be associated with the formation of threading screw dislocations that results in growth spirals if the films are grown at elevated temperatures. Such screw dislocations are observed in the large scale STM image shown in Fig. 2(d). (No such screw dislocations have been observed for the films grown at 200 °C.) Interestingly, the step height close to the growth spirals is only 0.3 nm, i.e., half-a-layer high, suggesting that at growth spirals, the growth proceeds via half a TMD layer that then converts into a full

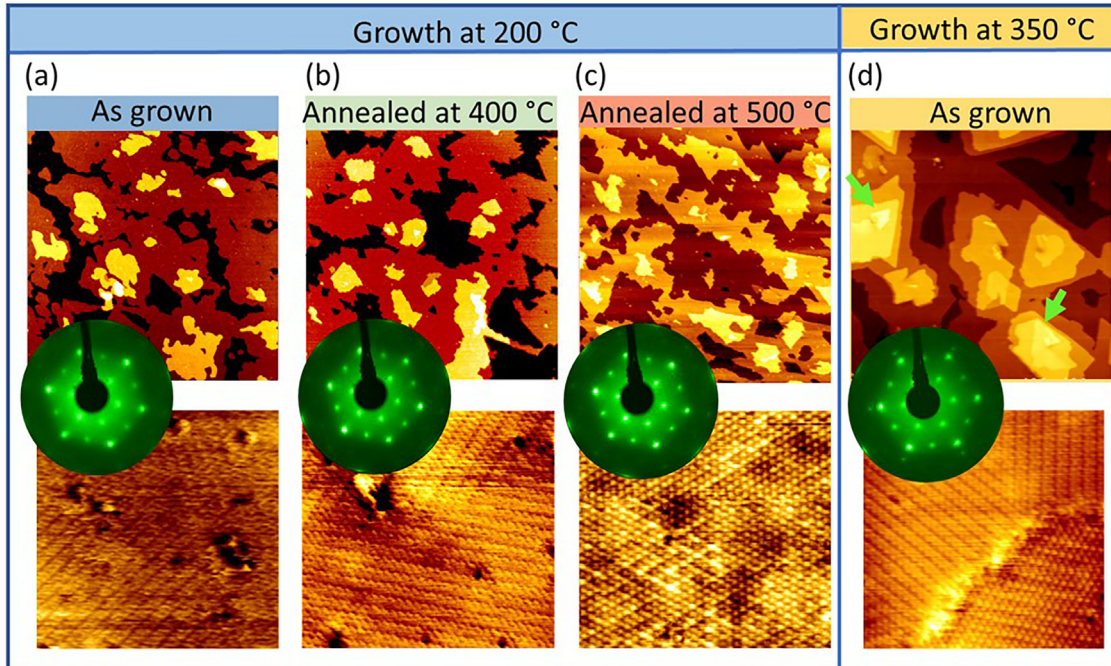


FIG. 2. Film morphology for different post-growth annealing temperatures and different growth temperatures. (a) Characteristic features of samples grown at 200 °C are large and flat terraces revealed by STM. Annealing of low temperature grown films results in terraces with straighter step edges (compared to the meandering edges of the as-grown film), whereas the overall topography does not change significantly. Annealing, however, does affect the atomic structure, which is reflected by reduction of the background intensity compared to the diffraction spot intensity in the LEED pattern and a change in the high-resolution STM images. The initially defective surface visible in atomic resolved STM images shows a more pronounced 2×1 corrugation upon annealing to 400 °C (b) and eventually changes its corrugation when the annealing temperature reaches 500 °C (c). The 2×1 periodicity almost completely disappears, and instead, a predominantly 1×1 pattern with small domains of 2×2 structures is observed. (d) Growth at elevated temperatures results in more terraces being exposed within the same sized area. The green arrows in (d) point to threading screw dislocations. On the atomic scale, less defects are observed, which is consistent with the sharp spots in LEED. All large scale (top row) and small scale (bottom row) STM images are $400 \times 400 \text{ nm}^2$ and $11 \times 11 \text{ nm}^2$ large, respectively. STM imaging conditions (sample bias, tunneling current): large scale -1.3 V , 0.7 nA ; small scale -0.1 V , 0.7 nA . All LEED data were acquired at room temperature with a primary electron energy of $E_k = 65 \text{ eV}$.

TMD layer with intercalated Cr as the spiral grows. More STM characterization of the growth spirals can be found in the [supplementary material](#), Sec. III.

B. Atomic structure and compositional analysis of thin $\text{Cr}_{(1+\delta)}\text{Te}_2$ films

Self-intercalation compounds can have different compositions of the intercalated layer, and in some recent studies, it has been shown that the composition can also be tuned by controlling the growth conditions.⁴⁰ In the $\text{Cr}_{(1+\delta)}\text{Te}_2$ samples grown here, a 2×1 structure is observed consistently, suggesting that in the growth and annealing range explored, here the films are closely related. Only at high annealing temperature, STM indicates the formation of 1×1 (with small 2×2 domains) structures that suggests the formation of a different intercalation compound. Generally, the Cr-Te phase diagram exhibits compositions with $\delta = 1/2$, $1/3$, or $1/4$ with the Cr atoms arranged in a 2×1 - $(\sqrt{3} \times \sqrt{3}) R30^\circ$, or 2×2 -periodicity, respectively, relative to the hexagonal 1×1 unit cell of a 1T-TMD layer. The 2×1 structure would imply that the films have a close to $\delta = 1/2$ Cr-layer in between the TMD layers (see Fig. 1). However, most reports of MBE grown $\text{Cr}_{(1+\delta)}\text{Te}_2$, albeit thicker films than those reported here, show a

preference for the $(\sqrt{3} \times \sqrt{3}) R30^\circ$ intercalation layer with a composition of $\delta = 1/3$.^{22,24} To assess the composition and structure of the film beyond the surface layer probed by STM and LEED, we performed high resolution RBS and GIXRD studies. The RBS analysis is outlined in detail in the [supplementary material](#). For films grown between 200 °C and 350 °C, RBS indicates atomic ratios of Cr:Te = 1.54 ± 0.10 : 2. (The uncertainty comes from a spread in values for different samples.) This ratio is closer to the stoichiometry of Cr_3Te_4 and, thus, consistent with the 2×1 structure. Annealing samples below 350 °C does not change the stoichiometry significantly, and annealing to above 400 °C is required to induce significant tellurium/chalcogen loss from the film.^{41,42} Samples annealed to 400 °C and 500 °C show an increased Cr:Te ratio to 2.05 ± 0.05 :2, i.e., the films are converted to a Cr monotelluride. In other words, all of the “intercalation layer” is close to fully occupied with Cr and, thus, δ is close to 1. Detailed structural analysis was also performed by GIXRD measurements for a sample grown at 350 °C. A detailed description of the measurements and analysis can be found in the [supplementary material](#). The GIXRD confirms the 2×1 structure. Structural refinement of a self-intercalated $\text{Cr}_{(1+\delta)}\text{Te}_2$ was carried out by comparing measured structure factor magnitudes to calculated values for the refined structures. Interestingly, while the intercalated Cr-atoms in a 2×1 structure are confirmed by GIXRD, a better agreement

between the measured and calculated structure factors can be obtained by varying the concentration of the 2×1 intercalation layer. Best agreement is obtained for $\delta = 0.38 \pm 0.05$ compared to the full occupation with $\delta = 0.5$. Given the more complex analysis of GIXRD data, compared to RBS measurements, compositional measurements by RBS are considered to be more reliable.

It may be unexpected that our experimentally determined amount of intercalated Cr is higher than the often cited preferred amount of $\delta = 1/3$. However, this may be justified in the ultrathin limit of our films and the lack of undercoordinated Cr-adatoms on the surface, i.e., only films terminated with a TMD layer and no “adsorbed” Cr-atoms are observed (see discussion below). As a consequence, a bilayer CrTe_2 with a single intercalation layer of $\delta = 1/3$ would have a film composition of $\text{Cr}:\text{Te} = 0.58$, i.e., less than the $\text{Cr}:\text{Te}$ ratio of $2/3$ as a bulk material with $\delta = 1/3$ has. With the increasing film thickness, the $\text{Cr}:\text{Te}$ ratio gets closer to the bulk value but since the surfaces remain Cr-deficient, the bulk value is never truly achieved. However, in these intercalation compounds, the $\text{Cr}:\text{Te}$ ratio can be also adjusted by changing the Cr-concentration in the intercalation layer and, thus, for ultrathin films, the assumedly preferred $2/3$ ratio can be obtained by increasing the Cr-content of the intercalation layer. For instance, an intercalation layer with $\delta = 1/2$, a preferred $\text{Cr}:\text{Te}$ ratio of $2/3$, is achieved for film thicknesses of 3–4 TMD layers. Thus, the combination of a preferred $\text{Cr}:\text{Te}$ ratio and the absence of energetically unfavorable undercoordinated Cr-atoms on top of the TMD layer at a surface may help to explain the experimentally observed larger than $1/3$ -Cr intercalation amount in ultrathin films.

C. Growth of quasi 2D $\text{Cr}_{(1+\delta)}\text{Te}_2$

STM measurements show that the $\text{Cr}_{(1+\delta)}\text{Te}_2$ films are terminated by a TMD layer with a 2×1 corrugation but no Cr-adatoms. Similarly, we previously published results from *ab initio* molecular dynamics simulations that demonstrated that Cr-atoms in between MoS_2 and a $\text{Cr}_{(1+\delta)}\text{Te}_2$ film are unstable and formation of a van der Waals gap is favored between the film and the vdW-substrate.¹² A sharp interface between intercalation compounds and MoS_2 substrate has also been previously supported by scanning transmission electron microscopy studies.¹² Such sharp vdW-interfaces are consistent with the vdW epitaxy growth described here. Thus, the termination of $\text{Cr}_{(1+\delta)}\text{Te}_2$ films with TMD layers at both the surface and its interface to MoS_2 makes them quasi vdW materials, and the thinnest form of this material is a bilayer TMD with a single intercalated Cr layer. Such a nanosheet may be considered a quasi 2D material with vdW surfaces. To explore this ultrathin limit for $\text{Cr}_{(1+\delta)}\text{Te}_2$, low temperature (200°C) growth was employed, which we have shown above to result in better layer-by-layer growth than growth at higher temperatures. Figure 3 shows STM images and a LEED pattern of such bilayer films. The LEED pattern shows an intense MoS_2 substrate and $\text{Cr}_{(1+\delta)}\text{Te}_2$ integer order reflections together with faint 2×1 superstructure reflections. The STM image reveals that the surface is predominantly covered with a bilayer $\text{Cr}_{(1+\delta)}\text{Te}_2$ with a step height of approximately 1.2 nm relative to the bare $\text{MoS}_2(0001)$ surface. On top of this bilayer film, some islands are seen that are 0.6 nm higher, i.e., these regions correspond to tri-layers TMDs. Interestingly, we observe also a few islands with an apparent elevation of 0.3 nm above the top of the bilayer

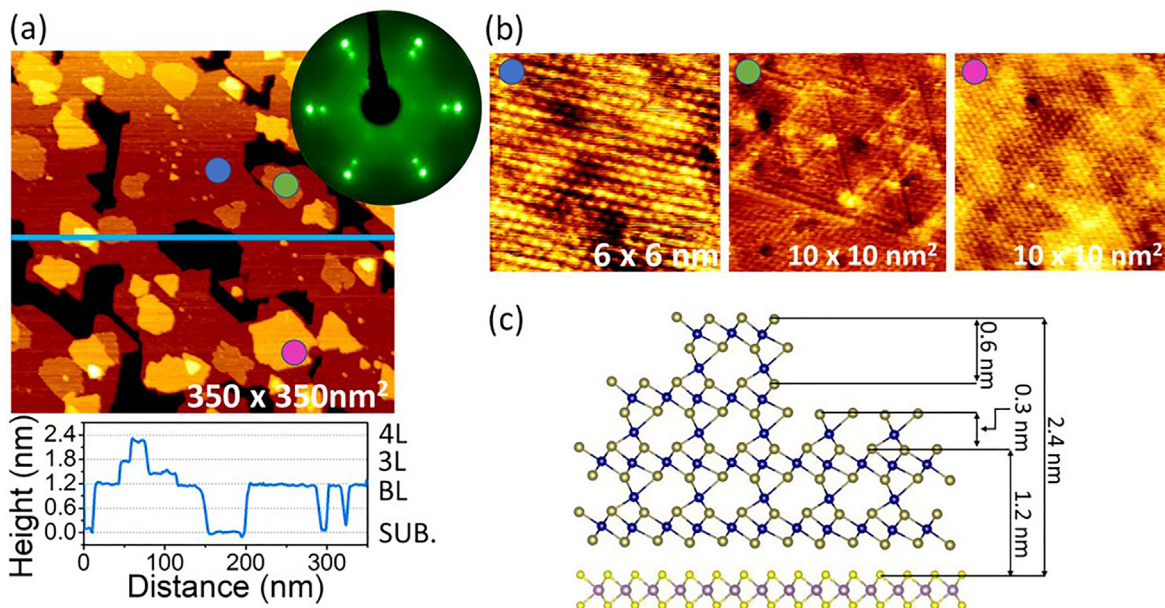


FIG. 3. Crystal structure, STM, and LEED characterization of a two TMD layer thick Cr-Te film grown on the MoS_2 substrate at 200°C . (a) Large scale STM image exhibiting large and atomically flat terraces. The profile along the blue line is shown below the image. The LEED diffraction pattern presents strong integer order diffraction reflections from the MoS_2 substrate in addition to the diffraction from the $\text{Cr}_{(1+\delta)}\text{Te}_2$ film. The 2×1 superlattice reflections are only faintly visible. The primary electron energy for the LEED pattern was $E_k = 60 \text{ eV}$. (b) Atomically resolved STM images of the bilayer film surface as well as of the trilayer islands exhibiting predominantly 1×1 periodicity with only weak contrast modulations related to intercalated Cr atoms. (c) Model of the film structure outlining the different step heights observed in the line profile of the large scale STM image shown in (a). STM imaging conditions (sample bias, tunneling current): (a) 1.2 V, 0.7 nA; (b) 5 mV, 0.9 nA. LEED image was acquired with a primary electron energy of $E_k = 60 \text{ eV}$.

$\text{Cr}_{(1+\delta)}\text{Te}_2$ film. This height is similar to the height observed in the growth spirals formed during high temperature growth of $\text{Cr}_{(1+\delta)}\text{Te}_2$ films shown in Fig. S6. We tentatively assign these islands to half a CrTe layer, on top of the $\text{Cr}_{(1+\delta)}\text{Te}_2$ bilayer, as schematically shown in the structure model in Fig. 3(c). These studies show that we can obtain a close to full layer coverage of bilayer of an intercalated $\text{Cr}_{(1+\delta)}\text{Te}_2$ by low temperature growth. Note that under these growth conditions, we are not observing a single layer CrTe₂ that would have close to 0.6 nm height above the substrate¹² and the thinnest layer is ~ 1.2 nm.

D. Magnetic characterization

The magnetic characterization of the samples was carried out by XMCD and VSM experiments. Figure 4 presents XMCD measurements of the Cr L_{2,3} absorption edge collected in the total electron yield detection mode. Additional VSM measurements are discussed in

the [supplementary material](#), Sec. VII. The main difference between XMCD and VSM is that VSM also shows a secondary magnetic phase that is likely induced in the MoS₂ substrate by Cr-diffusion and formation of a diluted semiconducting ferromagnet, which has been reported for doped TMDs.^{43–49}

The as-grown 5–7 TMD layer thick films are characterized by a strong magnetic anisotropy with out of plane easy axis of magnetization, see Figs. 4(a) and 4(c). For both growth temperatures, 200 °C and 350 °C, an almost square hysteresis loop is observed with the coercive field of $H_C = 0.5$ and 0.25 T, respectively. The Curie temperature (T_C), which is derived from the temperature derivative of the magnetization obtained after FC in an external field of $\mu_0 H = 6$ T, is equal to approximately 160 and 190 K for the samples grown at low and elevated temperatures, respectively, see Figs. 4(d) and 4(e). Post-growth annealing at 500 °C of the multilayer thick films grown at 200 °C results in a change in electronic and magnetic properties. UPS spectra, shown in

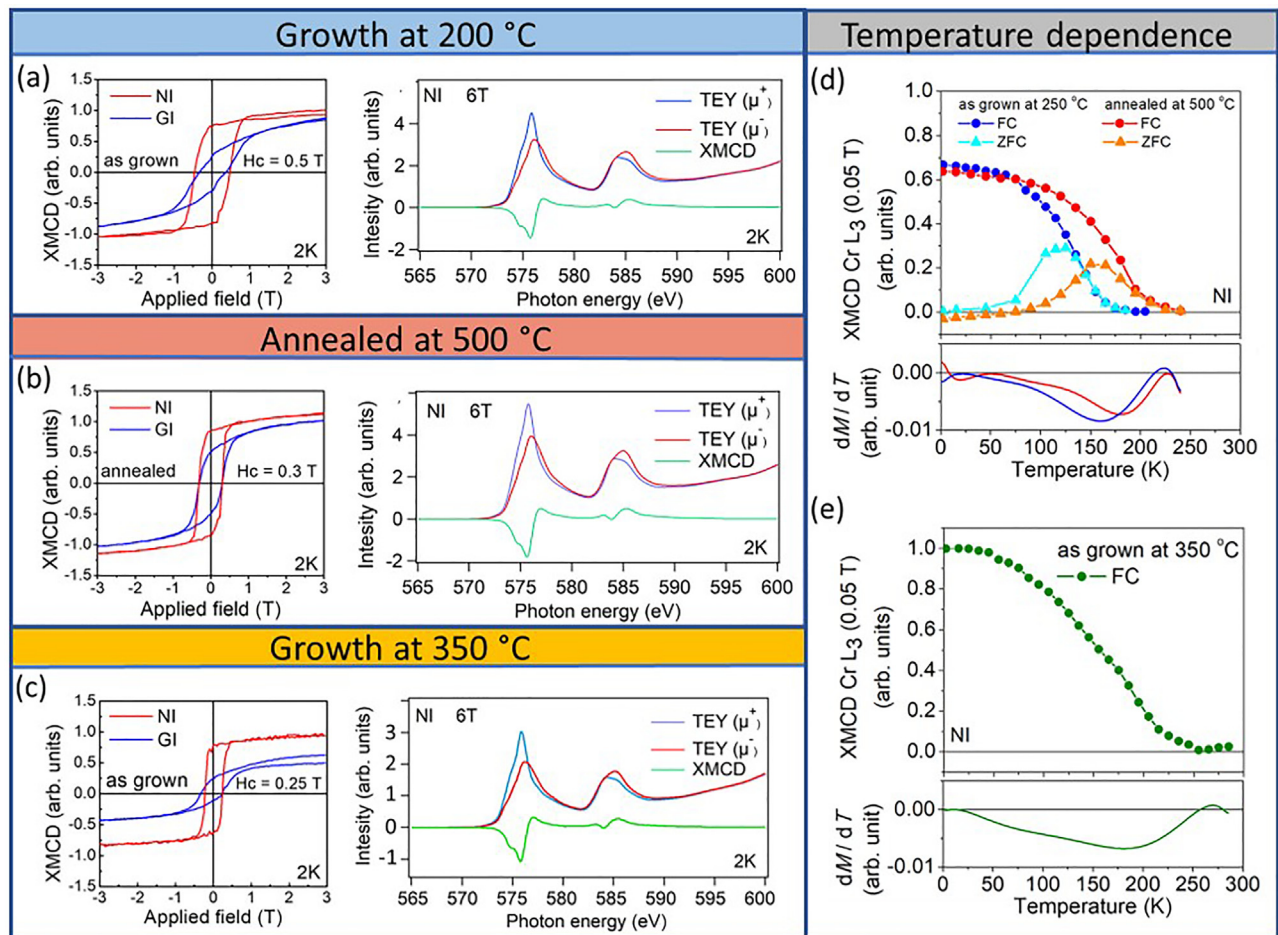


FIG. 4. Magnetic characterization of a 5–7 TMD-layer thick Cr-Te film. Measurements of element specific magnetization for Cr as a function of the applied magnetic field measured at 2 K for normal (NI) and grazing (70° relative to surface normal) (GI) x-ray incidence angle reveal strong anisotropy with out-of-plane easy axis of magnetization for samples grown at low as well as at elevated temperatures (a) and (c). Post-growth annealing (500 °C) of the sample grown at 200 °C results in an isotropization of the anisotropy energy (b). TEY spectra were carried out in a 50 mT field at normal incidence after zero field cooling and field cooling in 6 T applied field. (d) and (e) Temperature dependence of magnetization $M(T)$ reveals Curie temperature dependence on the growth and post-growth annealing temperature.

TABLE I. Orbital and spin magnetic moments of as-grown and annealed Cr-Te films.

	Growth at 350 °C	Growth at 200 °C	Annealed at 500 °C
m_s (μ_B/Cr)	3.65 ± 0.2	3.3 ± 0.2	3.45 ± 0.2
m_l (μ_B/Cr)	0.17 ± 0.01	0.14 ± 0.01	0.16 ± 0.01

Fig. S7, indicate a loss of spectral weight in the 0.5–1.5 eV binding energy window, while the Fermi-edge region is barely influenced by the compositional change. This suggests similar Cr 3d bands at the Fermi-level that are associated with itinerant magnetism in these materials. While this may indicate similar magnetic moments, we find that the compositional change affects their magnetic anisotropy. As can be seen from Fig. 4(b), the annealed film exhibits less of a preferential magnetization direction. Furthermore, H_C has decreased to 0.3 T, closely matching the coercive field observed for films grown at elevated temperatures. A similar trend has been observed for T_C , which is approximately 180 K, being very close to T_C observed for the samples grown at 350 °C. Strong bifurcation between ZFC and FC curves, observed in both as-grown and annealed samples [Fig. 4(d)], suggests the coexistence of ferromagnetic and antiferromagnetic coupling in the studied films. This hypothesis is in line with previous studies on the chromium telluride systems,^{50,51} which suggest large magnetic moment of the Cr atoms in the fully occupied layer, whereas the Cr atoms in the partially filled layers have only a small magnetic moment that points antiparallel to the moment of fully occupied layers.

Spin and orbital magnetic moments of Cr were derived from the sum rules (see the [supplementary material](#), Sec. V, for data analysis procedure) for the as-grown and annealed films and are listed in Table I. They do not significantly vary relative to each other within the uncertainty of the measurement.

Moreover, the two Cr species, i.e., Cr-atoms in the TMD layer and Cr-atoms in the intercalation layer, exhibit slightly different projected density of d- states as shown by DFT calculations

presented in Fig. S9. This may allow, in principle, a separation of the two species in high resolution XMCD and, thus, determination of their magnetic moments. While such a determination of the magnetic moments of the different Cr species would be desirable for determining magnetic coupling between the different species, the determination of the magnetic moments has not been possible in the data presented.

Most importantly, ferromagnetic order is maintained even when reducing the film thickness to the quasi 2D limit of a bi-layer TMD with a single Cr-intercalation layer. Figure 5(a) presents XMCD magnetization loops measured at 2 K with the external magnetic field applied in both normal incidence (NI) and grazing incidence (GI) directions. A bilayer thick film grown at 200 °C presents analogous magnetic behavior as presented above for multilayer film grown at the same temperature. The easy direction of magnetization is parallel to the *c* axis, and the coercive field is of about 0.5 T. Curie temperature estimated from the derivative of $M(T)$ field cooled curve [Fig. 5(b)] is about 150 K, which is only slightly lower than the T_C observed for multilayer samples grown under the same conditions. Values of magnetic moments per Cr atom decrease only slightly with the film thickness and are $m_s = 3.02 \pm 0.20 \mu_B$ and $m_l = 0.12 \pm 0.01 \mu_B$ for the bilayer film. The large magnetic moments in these films are consistent with the magnetism originating from the partially occupied d-electron orbitals. Such a partial occupation of the d-levels may allow a tuning of the magnetic properties by charge transfer doping. This may also be related to recent reports of inducing magnetism into non-magnetic Cr-selenide films by interface charge transfer.⁵² In our case, we probe the sensitivity of ultrathin films to electron doping by vacuum deposition of potassium as an efficient electron donor. Figure 5(c) shows the XMCD signal before and after potassium deposition. Using the sum rule, we calculate the magnetic moments and a decrease in the magnetization by $\sim 20\%$ is observed after electron doping by potassium adsorption. Moreover, potassium adsorption induces a reduction of T_C by ~ 15 K. This demonstrates that filling the d-levels in this material causes a decrease in the spin polarized states and the magnetic properties can be tuned in these quasi-2D materials by external charge doping.

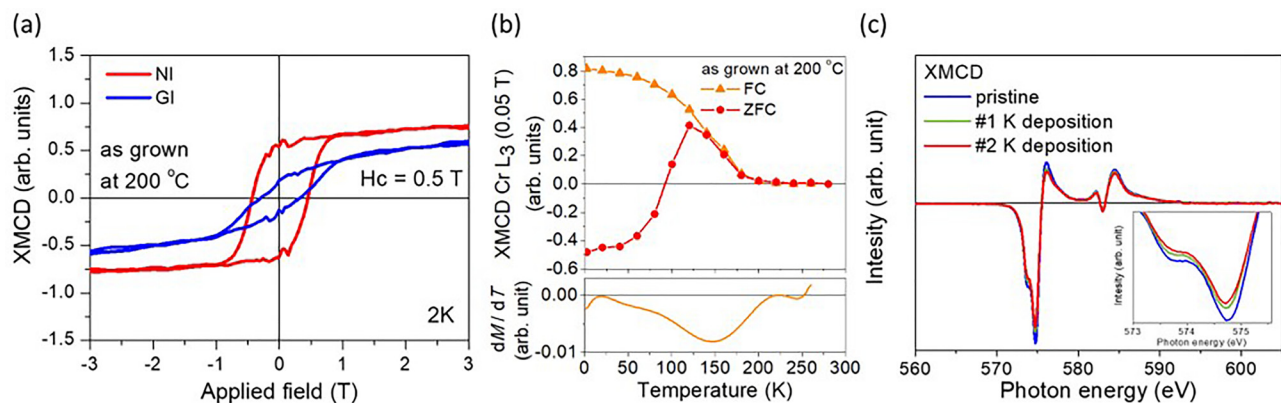


FIG. 5. Magnetic characterization of a two TMD layer thick Cr-Te film with a single Cr-intercalation layer. (a) Element specific magnetization of Cr vs external magnetic field measured at 2 K under normal and grazing x-ray incidence condition. (b) Temperature dependence of magnetization measured in a 50 mT applied field at normal x-ray incidence after ZFC and FC preparation in 6 T. (c) Variation of the XMCD signal with potassium deposition (electron doping). Two potassium depositions (nos. 1 and 2) were carried out with the largest change obtained after the first deposition. The XMCD signal decreases with potassium deposition by $\sim 20\%$, which is more clearly seen in the zoomed in image shown in the inset.

IV. DISCUSSION

Ultrathin $\text{Cr}_{(1+\delta)}\text{Te}_2$ films forming a 2×1 structure are prepared by MBE growth on the (0001) surface of MoS_2 at temperatures between 200°C and 350°C . The experimentally observed preference of the 2×1 structure in ultrathin films over the more frequently discussed $(\sqrt{3} \times \sqrt{3})$ $R30^\circ$ structure with $\delta = 1/3$ is supported by DFT calculations. Below a thickness of about 20 TMD layers, the stabilization of the 2×1 Cr-self-intercalation layer is a consequence of a lower surface energy compared to that of the $(\sqrt{3} \times \sqrt{3})$ $R30^\circ$ structure. Thus, this observation suggests that $\text{Cr}_{(1+1/3)}\text{Te}_2$ also undergoes a layer dependent structural transition from a $(\sqrt{3} \times \sqrt{3})$ $R30^\circ$ structure in the bulk to a (defective) 2×1 structure below approximately 20 TMD layers. These structural transitions may also be responsible for reported unusual layer dependent magnetic transition with higher T_c 's for thinner CVD grown films.²⁸ In the study here, we are, however, always in the ultrathin limit that favors the 2×1 ordering.

All films studied here are ferromagnetic, but some interesting variations of the magnetic properties depending on sample preparation have been observed. Samples that exhibit a 2×1 structure also exhibiting strongly anisotropic magnetic properties with an easy axis along the *c*-axis (out-of-plane) and a Curie temperature between 160 and 190 K for multilayers. Importantly, the magnetic properties of the films remain almost unaltered even if the film thickness is reduced to the pseudo 2D limit of a bilayer of CrTe_2 with a single intercalation layer. Only a small reduction of T_c is observed, which may be a consequence of the reduced dimension of the film or a small variation of the amount of intercalated Cr.

For the multilayers, the magnetic properties can be tuned by the variation of the post growth annealing temperature. STM of post-growth annealed films indicates a gradual loss of long range order of the superstructure, while RBS measurements indicate an increase in the Cr:Te ratio up to a value close to 1:1. This is consistent with an increase in the concentration of intercalated Cr because of Te-loss during high temperature annealing and the formation of a Cr-monotelluride film. Such modified films are characterized by an increased T_c , a coercive field being reduced from 0.5 to 0.3 T, and an isotropization of the magnetic anisotropy. We consider that the change in the magnetic anisotropy is directly related to the change in structural anisotropy due to the occupation of a larger fraction of intercalation sites. High temperature annealing also leads to a reduction in the defect concentration in the CrTe_2 TMD layers and to an enhancement of the long-range order (as evident by a background reduction of the LEED pattern and the sharpening of the reflections). The better ordering may cause the reduction of the coercive field strength. A similar reduction of H_c is observed for films grown at higher temperatures that also show better ordering as evident by LEED and STM. In contrast to the post-growth annealed samples, samples grown at 350°C exhibit a well-ordered 2×1 structure in STM images suggesting a close to $\delta = 0.5$ occupation of the intercalation layer. This is consistent with the persistence of the strong out-of-plane magnetic anisotropy.

The magnetism estimated from XMCD indicates a large magnetic moment per Cr atom of above $3 \mu_B$ per Cr-atom. This is consistent with itinerant magnetism originating from the partially occupied *d*-electrons, and this suggests that the magnetism may be tuned by altering the electron occupation. Charge transfer doping by potassium deposition reveals a suppression of the magnetism in bilayer films; this

may suggest that to enhance magnetism modification of the ultrathin film the use of an electron acceptor should be explored. Also, strong field effect, such as possible in ion-liquid gating, may allow tuning the magnetic properties in this material and this should be explored in future studies by transport measurements.

V. CONCLUSIONS

In conclusion, although progress has been made in identifying 2D ferromagnetic vdW materials, most of them exhibit low Curie temperatures and are difficult to be grown as thin films, which makes it difficult to deploy them in scalable processes. Here, we demonstrated that self-intercalated $\text{Cr}_{(1+\delta)}\text{Te}_2$ can be an alternative to pure vdW materials for a bottom-up growth of vdW heterostructures (here, $\text{Cr}_{(1+\delta)}\text{Te}_2/\text{MoS}_2$). $\text{Cr}_{(1+\delta)}\text{Te}_2$ can be grown with vdW interfaces due to the termination of the material with a TMD layer. $\text{Cr}_{(1+\delta)}\text{Te}_2$ compounds are known to be ferromagnetic in the bulk, and our studies showed that these ferromagnetic properties are maintained down to its ultrathin limit, consisting of only two TMD layers and a single layer of intercalated Cr. This makes this an ultrathin, quasi-2D ferromagnet, which can be grown on other vdW materials and maintain a vdW gap at the interface.¹² The magnetic properties of this material are only weakly affected by film thickness or growth conditions, thus making it a robust ferromagnetic material with relatively high T_c and, therefore, an ideal material for MBE synthesis of vdW heterostructures. The tunability of the magnetic properties of $\text{Cr}_{(1+\delta)}\text{Te}_2$ by the amount of intercalated Cr may be extended by alloying with other transition metals, and this will be explored in future experiments to increase the T_c to above RT. Our results should pave the way for the investigation of ferromagnetic vdW heterostructures prepared by direct growth methods.

SUPPLEMENTARY MATERIAL

See the [supplementary material](#) for more information that supports the findings of this study, including STM characterization of growth spirals for films grown at 350°C ; a detailed description of structural and compositional analysis by grazing incidence x-ray diffraction and Rutherford Backscattering Spectroscopy; description of magnetic modifications of MoS_2 (comparison XMCD vs VSM), description of magnetic moment evaluation from XMCD measurements and the ultraviolet photoemission spectroscopy measurements of the as-grown and annealed Cr-Te films; and PDOS calculations for Cr-atoms in two different lattice sites.

ACKNOWLEDGMENTS

The USF group acknowledges support from the National Science Foundation under Award No. DMR-2118414. Numerical calculations were supported in part by ICM, at Warsaw University under Grant No. GB84-36. The XAS/XMCD experiments were performed at BOREAS beamline at ALBA Synchrotron with the collaboration of ALBA staff.

AUTHOR DECLARATIONS

Conflict of Interest

The authors have no conflicts to disclose.

DATA AVAILABILITY

The data that support the findings of this study are available within the article and its [supplementary material](#).

REFERENCES

- ¹K. S. Burch, D. Mandrus, and J.-G. Park, "Magnetism in two-dimensional van der Waals materials," *Nature* **563**, 47 (2018).
- ²C. Gong and X. Zhang, "Two-dimensional magnetic crystals and emergent heterostructure devices," *Science* **363**, eaav4450 (2019).
- ³H. Li, S. Ruan, and Y.-J. Zeng, "Intrinsic van der Waals magnetic materials from bulk to the 2D limit: New frontiers of spintronics," *Adv. Mater.* **31**, 1900065 (2019).
- ⁴K. Lasek, J. Li, S. Kolekar, P. M. Coelho, M. Zhang, Z. Wang, and M. Batzill, "Synthesis and characterization of 2D transition metal dichalcogenides: Recent progress from a vacuum surface science perspective," *Surf. Sci. Rep.* **76**, 100523 (2021).
- ⁵A. Koma, K. Sunouchi, and T. Miyajima, "Fabrication of ultrathin heterostructures with van der Waals epitaxy," *J. Vac. Sci. Technol. B* **3**, 724 (1985).
- ⁶K. Saiki, K. Ueno, T. Shimada, and A. Koma, "Application of van der Waals epitaxy to highly heterogeneous systems," *J. Cryst. Growth* **95**, 603 (1989).
- ⁷X. Yuan, L. Tang, S. Liu, P. Wang, Z. Chen, C. Zhang, Y. Liu, W. Wang, Y. Zou, C. Liu, N. Guo, J. Zou, P. Zhou, W. Hu, and F. Xiu, "Arrayed van der Waals vertical heterostructures based on 2D GaSe grown by molecular beam epitaxy," *Nano Lett.* **15**, 3571 (2015).
- ⁸L. A. Walsh and C. L. Hinkle, "Van der Waals epitaxy: 2D materials and topological insulators," *Appl. Mater. Today* **9**, 504 (2017).
- ⁹Y. J. Hong, W. H. Lee, Y. Wu, R. S. Ruoff, and T. Fukui, "van der Waals epitaxy of InAs nanowires vertically aligned on single-layer graphene," *Nano Lett.* **12**, 1431 (2012).
- ¹⁰J. Kim, C. Bayram, H. Park, C.-W. Cheng, C. Dimitrakopoulos, J. A. Ott, K. B. Reuter, S. W. Bedell, and D. K. Sadana, "Principle of direct van der Waals epitaxy of single-crystalline films on epitaxial graphene," *Nat. Commun.* **5**, 4836 (2014).
- ¹¹P. Periwal, J. D. Thomsen, K. Reidy, G. Varnavides, D. N. Zakharov, L. Gignac, M. C. Reuter, T. J. Booth, S. Hofmann, and F. M. Ross, "Catalytically mediated epitaxy of 3D semiconductors on van der Waals substrates," *Appl. Phys. Rev.* **7**, 031402 (2020).
- ¹²K. Lasek, P. M. Coelho, K. Zberecki, Y. Xin, S. K. Kolekar, J. Li, and M. Batzill, "Molecular beam epitaxy of transition metal (Ti-, V-, and Cr-) tellurides: From monolayer ditellurides to multilayer self-intercalation compounds," *ACS Nano* **14**, 8473 (2020).
- ¹³Y. Fujisawa, M. Pardo-Almanza, J. Garland, K. Yamagami, X. Zhu, X. Chen, K. Araki, T. Takeda, M. Kobayashi, Y. Takeda, C. H. Hsu, F. C. Chuang, R. Laskowski, K. H. Khoo, A. Soumyanarayanan, and Y. Okada, "Tailoring magnetism in self-intercalated Cr_{1+x}Te₂ epitaxial films," *Phys. Rev. Mater.* **4**, 114001 (2020).
- ¹⁴D. C. Freitas, R. Weht, A. Sulpice, G. Remenyi, P. Strobel, F. Gay, J. Marcus, and M. Núñez-Regueiro, "Ferromagnetism in layered metastable 1T-CrTe₂," *J. Phys.: Condens. Matter* **27**, 176002 (2015).
- ¹⁵X. Zhang, Q. Lu, W. Liu, W. Niu, J. Sun, J. Cook, M. Vaninger, P. F. Miceli, D. J. Singh, S.-W. Lian, T.-R. Chang, X. He, J. Du, L. He, R. Zhang, G. Bian, and Y. Xu, "Room-temperature intrinsic ferromagnetism in epitaxial CrTe₂ ultrathin films," *Nat. Commun.* **12**, 2492 (2021).
- ¹⁶L. Meng, Z. Zhou, M. Xu, S. Yang, K. Si, L. Liu, X. Wang, H. Jiang, B. Li, P. Qin, and P. Zhang, "Anomalous thickness dependence of Curie temperature in air-stable two-dimensional ferromagnetic 1T-CrTe₂ grown by chemical vapor deposition," *Nat. Commun.* **12**, 809 (2021).
- ¹⁷A. Purbawati, J. Coraux, J. Vogel, A. Hadj-Azzem, N. Wu, N. Bendiab, D. Jegouso, J. Renard, L. Marty, V. Bouchiat, A. Sulpice, L. Aballe, M. Foerster, F. Genuzio, A. Locatelli, T. O. Menteş, Z. V. Han, X. Sun, M. Núñez-Regueiro, and N. Rougemaille, "In-plane magnetic domains and Néel-like domain walls in thin flakes of the room temperature CrTe₂ Van der Waals ferromagnet," *ACS Appl. Mater. Interfaces* **12**, 30702 (2020).
- ¹⁸X. Yang, X. Zhou, W. Feng, and Y. Yao, "Tunable magneto-optical effect, anomalous Hall effect, and anomalous Nernst effect in the two-dimensional room-temperature ferromagnet 1T-CrTe₂," *Phys. Rev. B* **103**, 024436 (2021).
- ¹⁹X. Sun, W. Li, X. Wang, Q. Sui, T. Zhang, Z. Wang, L. Liu, D. Li, S. Feng, S. Zhong, and H. Wang, "Room temperature ferromagnetism in ultra-thin van der Waals crystals of 1T-CrTe₂," *Nano Res.* **13**, 3358 (2020).
- ²⁰G. Chattopadhyay, "The Cr-Te (chromium-tellurium) system," *J. Phase Equilib.* **15**, 431 (1994).
- ²¹L.-Z. Zhang, X.-D. He, A.-L. Zhang, Q.-L. Xiao, W.-L. Lu, F. Chen, Z. Feng, S. Cao, J. Zhang, and J.-Y. Ge, "Tunable Curie temperature in layered ferromagnetic Cr_{5+x}Te₈ single crystals," *APL Mater.* **8**, 031101 (2020).
- ²²D. M. Burn, L. B. Duffy, R. Fujita, S. L. Zhang, A. I. Figueroa, J. Herrero-Martin, G. van der Laan, and T. Hesjedal, "Cr₂Te₃ thin films for integration in magnetic topological insulator heterostructures," *Sci. Rep.* **9**, 10793 (2019).
- ²³M. G. Sreenivasan, X. J. Hou, K. L. Teo, M. B. Jalilb, A. Liew, and T. C. Chong, "Growth of CrTe thin films by molecular-beam epitaxy," *Thin Solid Films* **505**, 133 (2006).
- ²⁴A. Roy, S. Guchhait, R. Dey, T. Pramanik, C.-C. Hsieh, A. Rai, and S. K. Banerjee, "Perpendicular magnetic anisotropy and spin glass-like behavior in molecular beam epitaxy grown chromium telluride thin films," *ACS Nano* **9**, 3772 (2015).
- ²⁵R. Chua, J. Zhou, X. Yu, W. Yu, J. Gou, R. Zhu, L. Zhang, M. B. H. Breese, W. Chen, K. P. Loh, Y. P. Feng, M. Yang, Y. L. Huang, and A. T. S. Wee, "Room temperature ferromagnetism of monolayer chromium telluride with perpendicular magnetic anisotropy," *Adv. Mater.* **33**, 2103360 (2021).
- ²⁶L. Hui, S. Lim, J. Bi, and K. Teo, "Investigation on the antiferromagnetic component in the intrinsic exchange bias in structurally single phase Cr₂Te₃ thin film," *J. Appl. Phys.* **111**, 07D719 (2012).
- ²⁷H. Li, L. Wang, J. Chen, T. Yu, L. Zhou, Y. Qiu, H. He, F. Ye, I. K. Sou, and G. Wang, "Molecular beam epitaxy grown Cr₂Te₃ thin films with tunable Curie temperatures for spintronic devices," *ACS Appl. Nano Mater.* **2**, 6809 (2019).
- ²⁸Y. Wen, Z. Liu, Y. Zhang, C. Xia, B. Zhai, X. Zhang, G. Zhai, C. Shen, P. He, R. Cheng, and L. Yin, "Tunable room-temperature ferromagnetism in two-dimensional Cr₂Te₃," *Nano Lett.* **20**, 3130 (2020).
- ²⁹I. H. Lee, B. K. Choi, H. J. Kim, M. J. Kim, H. Y. Jeong, J. H. Lee, S.-Y. Park, Y. Jo, C. Lee, J. W. Choi, S. W. Cho, S. Lee, Y. Kim, B. H. Kim, K. J. Lee, J. E. Heo, S. H. Chang, F. Li, B. L. Chittari, J. Jung, and Y. J. Chang, "Modulating Curie temperature and magnetic anisotropy in nanoscale-layered Cr₂Te₃ films: Implications for room-temperature spintronics," *ACS Appl. Nano Mater.* **4**, 4810 (2021).
- ³⁰A. Barla, J. Nicolás, D. Cocco, S. M. Valvidares, J. Herrero-Martín, P. Gargiani, J. Moldes, C. Ruget, E. Pellegrin, and S. Ferrer, "Design and performance of BOREAS, the beamline for resonant x-ray absorption and scattering experiments at the ALBA synchrotron light source," *J. Synchrotron Radiat.* **23**, 1507 (2016).
- ³¹G. Kresse and J. Hafner, "Ab initio molecular dynamics for liquid metals," *Phys. Rev. B* **47**, 558 (1993).
- ³²G. Kresse and J. Hafner, "Ab initio molecular-dynamics simulation of the liquid-metal-amorphous-semiconductor transition in germanium," *Phys. Rev. B* **49**, 14251 (1994).
- ³³G. Kresse and J. Furthmüller, "Efficiency of ab-initio total energy calculations for metals and semiconductors using a plane-wave basis set," *Comput. Mater. Sci.* **6**, 15 (1996).
- ³⁴G. Kresse and J. Furthmüller, "Efficient iterative schemes for ab initio total-energy calculations using a plane-wave basis set," *Phys. Rev. B* **54**, 11169 (1996).
- ³⁵P. E. Blöchl, "Projector augmented-wave method," *Phys. Rev. B* **50**, 17953 (1994).
- ³⁶G. Kresse and D. Joubert, "From ultrasoft pseudopotentials to the projector augmented-wave method," *Phys. Rev. B* **59**, 1758 (1999).
- ³⁷J. P. Perdew, K. Burke, and M. Ernzerhof, "Generalized gradient approximation made simple," *Phys. Rev. Lett.* **77**, 3865 (1996).
- ³⁸T. Böker, R. Severin, A. Müller, C. Janowitz, R. Manzke, D. Voß, P. Krüger, A. Mazur, and J. Pollmann, "Band structure of MoS₂, MoSe₂, and α-MoTe₂: Angle-resolved photoelectron spectroscopy and ab initio calculations," *Phys. Rev. B* **64**, 235305 (2001).
- ³⁹M. Yamaguchi and T. Hashimoto, "Magnetic properties of Cr₃Te₄ in ferromagnetic region," *J. Phys. Soc. Jpn.* **32**, 635 (1972).
- ⁴⁰X. Zhao, P. Song, C. Wang, A. C. Riis-Jensen, W. Fu, Y. Deng, D. Wan, L. Kang, S. Ning, J. Dan, T. Venkatesan, Z. Liu, W. Zhou, K. S. Thygesen, X. Luo, S. J. Pennycook, and K. P. Loh, "Engineering covalently bonded 2D layered materials by self-intercalation," *Nature* **581**, 171 (2020).
- ⁴¹M. Bonilla, S. Kolekar, J. Li, Y. Xin, P. M. Coelho, K. Lasek, K. Zberecki, D. Lizzit, E. Tosi, P. Lacovig, S. Lizzit, and M. Batzill, "Compositional phase

- change of early transition metal diselenide (VSe₂ and TiSe₂) ultrathin films by postgrowth annealing," *Adv. Mater. Interfaces* **7**, 2000497 (2020).
- ⁴²J. Li, S. Kolekar, Y. Xin, P. M. Coelho, K. Lasek, F. A. Nugera, H. R. Gutierrez, and M. Batzill, "Thermal phase control of two-dimensional Pt-chalcogenide (Se and Te) ultrathin epitaxial films and nanocrystals," *Chem. Mater.* **33**, 8018 (2021).
- ⁴³S. Fu, K. Kang, K. Shayan, A. Yoshimura, S. Dadras, X. Wang, L. Zhang, S. Chen, N. Liu, A. Jindal, X. Li, A. N. Pasupathy, A. N. Vamivakas, V. Meunier, S. Strauf, and E.-H. Yang, "Enabling room temperature ferromagnetism in monolayer MoS₂ via in situ iron-doping," *Nat. Commun.* **11**, 2034 (2020).
- ⁴⁴P. M. Coelho, H. P. Komsa, K. Lasek, V. Kalappattil, J. Karthikeyan, M. H. Phan, A. V. Krasheninnikov, and M. Batzill, "Room-temperature ferromagnetism in MoTe₂ by post-growth incorporation of vanadium impurities," *Adv. Electron. Mater.* **5**, 1900044 (2019).
- ⁴⁵Y. Zhao, Y. Li, M. Liu, K. Xu, and F. Ma, "Strain-controllable phase and magnetism transitions in re-doped MoTe₂ monolayer," *J. Phys. Chem. C* **124**, 4299 (2020).
- ⁴⁶B. Song, S. J. Yun, J. Jiang, K. Beach, W. Choi, Y.-M. Kim, H. Terrones, Y. J. Song, D. L. Duong, and Y. H. Lee, "Evidence of itinerant holes for long-range magnetic order in tungsten diselenide semiconductor with vanadium dopants," *Phys. Rev. B* **103**, 094432 (2021).
- ⁴⁷Z. Guguchia, A. Kerelsky, D. Edelberg, S. Banerjee, F. von Rohr, D. Scullion, M. Augustin, M. Scully, D. A. Rhodes, Z. Shermadini, H. Luetkens, A. Shengelaya, C. Baines, E. Morenzoni, A. Amato, J. C. Hone, R. Khasanov, S. J. L. Billinge, E. Santos, A. N. Pasupathy, and Y. J. Uemura, "Magnetism in semiconducting molybdenum dichalcogenides," *Sci. Adv.* **4**, eaat3672 (2018).
- ⁴⁸S. J. Yun, D. L. Duong, D. M. Ha, K. Singh, T. L. Phan, W. Choi, Y.-M. Kim, and Y. H. Lee, "Ferromagnetic order at room temperature in monolayer WSe₂ semiconductor via vanadium dopant," *Adv. Sci.* **7**, 1903076 (2020).
- ⁴⁹F. Zhang, B. Zheng, A. Sebastian, D. H. Olson, M. Liu, K. Fujisawa, Y. T. H. Pham, V. O. Jimenez, V. Kalappattil, L. Miao, T. Zhang, R. Pendurthi, Y. Lei, A. L. Elías, Y. Wang, N. Alem, P. E. Hopkins, S. Das, V. H. Crespi, M. H. Phan, and M. Terrones, "Monolayer vanadium-doped tungsten disulfide: A room-temperature dilute magnetic semiconductor," *Adv. Sci.* **7**, 2001174 (2020).
- ⁵⁰T. Hamasaki, T. Hashimoto, Y. Yamaguchi, and H. Watanabe, "Neutron diffraction study of Cr₂Te₃ single crystal," *Solid State Commun.* **16**, 895 (1975).
- ⁵¹A. F. Andresen, E. Zeppezauer, T. Boive, B. Nordström, and C. Brändén, "Magnetic structure of Cr₂Te₃, Cr₃Te₄, and Cr₅Te₆," *Acta. Chem. Scand.* **24**, 3495 (1970).
- ⁵²B. Li, Z. Wan, C. Wang, P. Chen, B. Huang, X. Cheng, Q. Qian, J. Li, Z. Zhang, G. Sun, B. Zhao, H. Ma, R. Wu, Z. Wei, Y. Liu, L. Liao, Y. Ye, Y. Huang, X. Xu, X. Duan, W. Ji, and X. Duan, "Van der Waals epitaxial growth of air-stable CrSe₂ nanosheets with thickness-tunable magnetic order," *Nat. Mater.* **20**, 818 (2021).